Hindawi
Journal of Renewable Energy
Volume 2023, Article ID 3911228, 16 pages
https://doi.org/10.1155/2023/3911228

Research Article

CFD Simulations and Experimental Investigation of a Flat-Plate Solar Air Heater at Different Positions of Inlet and Outlet

Tigabu Mekonnen Belay and Samson Mekbib Atnaw

Mechanical Engineering, Addis Ababa Science and Technology University, Addis Ababa, Ethiopia

Correspondence should be addressed to Tigabu Mekonnen Belay; tigabu.mekonnen@aastustudent.edu.et

Received 14 August 2022; Revised 6 August 2023; Accepted 27 September 2023; Published 6 October 2023

Academic Editor: Wei-Hsin Chen

In this study, the effects of the positions of inlet and outlet in a single-flow flat plate rectangular box active solar air heater due to convective heat transfer were designed, constructed, theoretically investigated using CFD fluid flow (fluent) software, and experimentally examined. The internal dimensions of the solar air heater are length and width of 100 cm and 50 cm, respectively, and the air gap between absorber plate and glazing glass is 9 cm. The solar air heaters are constructed with 18 mm thickness plywood, 4 mm thickness glazing glass, and 1 mm thickness aluminium sheet metal. Except for the glazing glass, other construction materials are painted black to absorb solar radiation. The positions of the inlet and outlet depend on the fraction of the width of the solar air heater. Based on the three-day average outlet temperature of the solar air heaters, solar air heater B has the highest average outlet temperature compared with other active solar air heaters and ambient air temperatures. Based on the three-day average outlet temperature of solar air heaters and ambient air temperatures, the active solar air heater B outlet temperature is 33.83 percent greater than the ambient air average temperature. The average outlet temperature of the air in passive solar air heaters increased by 17% and 4.43% compared to ambient air and active solar air heaters outlet air temperatures, respectively, due to the speed of the air in the solar air heater. The uncertainty of the instruments to measure the temperature of the air is $\pm$ 0.289°C, and the uncertainty of the solar air heater is $\pm$ 0.462°C. A higher average air outlet temperature was achieved in March at a tilt angle of 12° at a latitude of 8.89°. The negative tilt angle in May at a latitude of 8.89° indicates the south-facing orientation of solar air heaters is better. The passive solar air heater and ambient air temperature have a higher air temperature fluctuation than the active solar air collector.

1. Introduction

The solar convection drying system is used to preserve fruits, vegetables, grains, fish, meat, and other agricultural products, which are free and renewable sources of energy [1]. In our solar system, the sun is the primary energy producer, in which a tremendous amount of energy is generated due to nuclear fusion taking place in its core. To make life possible on our planet, a small fraction of the energy generated by the sun hits the earth. Solar radiation is the cause of all natural cycles and activities like wind, rain, photosynthesis, ocean currents, and other phenomena that are important for life. The solar surface temperature of the sun is 6000°C, which corresponds from 70,000 to 80,000 kW/m^2 radiation intensity. From this amount of energy, the earth receives small portions, but when it is compared with the yearly energy demand of the whole world, it is more than 10,000 times. The solar radiation intensity or solar constant outside the atmosphere is 1,360 W/m^2, but when it penetrates the atmosphere, there is a loss on a clear sky on a sunny day in summer the global radiation obtained on the ground is between 800 and 1000W/m^2. The solar air heater absorbs the coming solar radiation. It is used to convert solar radiation into heat, directly into heat at the absorbing surface, and to transfer this heat into a fluid, either air or fluid [1]. 99.99% of the world energy source is derived from the sun [2]. Solar air heaters (SAHs) are low-cost devices that gather solar energy and distribute heated air at low to moderate temperatures for space heating, drying agricultural items such as fruits, seeds, and vegetables, and in some industrial applications [3]. Solar

thermal system converts the absorbed solar energy into heat rather than electricity [4]. For drying, advanced solar air collectors are commonly used in research [5].

Several types of solar air heaters, each with their unique temperature range, were illustrated [6]. Flat-plate solar collectors are widely utilised in low-temperature energy technologies, and they have attracted the interest of many researchers [7]. The flat-plate solar air heater is popularly used in solar dryer systems. These collectors heat liquid or air at temperatures less than 80℃. In other circumstances, an average efficiency of less than 25% was projected during the experimental development of solar air heaters for unconventional air, but an average efficiency of 28.7% was obtained [8, 9]. The flat-plate collector benefits the most from the double pass mode, while the v-groove collector benefits the least [10]. A solar air heater is typically used in indirect or hybrid active or passive solar dryers to heat the air before it enters the drying chamber [11]. Among the reported types of solar dryers, the indirect-mode forced convection solar dryer is superior in drying speed and quality of drying [12]. Active solar dryers (also known as hybrid solar drying systems) use ventilation to circulate heated air either within the drying chamber or from the solar air heater to the drying chamber [13]. Moreover, drying using a fan may achieve the same output as a natural convection solar dryer with a heater area of six times as large [1].

In the analysis of the performance of solar air heaters, different modifications are required. In solar thermal system applications, the solar air heater is the most crucial device. The drying of agricultural products and the heating of houses are two of the most common uses for solar air heaters. It has a basic design, requires less care, and is less expensive than other solar heaters [14]. It is critical for performance enhancement [12]. Solar air heaters' thermal performance is influenced by their material, shape, dimension, fin [3, 15, 16], phase change material [14], tilt angle [17], air gap [18], and glazing thickness [19].

Another factor that was studied in this research is the four different positions of the inlet and outlet of the rectangular solar air heater. Different positions and features of the inlet and outlet of the solar air collector are used in different research. As an example, a rectangular inlet with an equal cross-section area and a diverging outlet [20], an inlet and outlet at the side of the solar air heaters [15], a box-type with an equal rectangular inlet and outlet having similar dimensions to the cross-section area [21, 22], a box-type with two inlets and one exit [23], a two-pass rectangular box type [24], a converged inlet and a normal rectangular cross-section outlet [11], with a double pass [25], and other position of inlet and outlet. In this study, the effect of the positions of the inlet and outlet of the rectangular solar air heater was studied for the following reasons: to look into the effects of different positions on the inlet and outlet of a solar air heater, to check the angle of the solar air heater on the south face of the north hemisphere from the horizontal centroid line, to compare the active and passive solar air heater outlet temperatures, to examine several designs for uniform air flow and temperature distribution using CFD and experimental testing for various solar air heaters, and to fabricate and evaluate the optimum design by comparing experimental and CFD data. Convective heat transfer is a basic term that has great importance in thermal performance analysis in different applications such as heating and cooling. Starting from the initial stage of heating the air in the solar air heater to remove the moisture from the product inside the drying chamber is based on the principle of convective heat transfer. In this study, the importance of convective heat transfer in solar air heaters at different positions of inlet and outlet and the effect of convective heat transfer with respect to the contact time that affects the outlet temperature of the solar air heater at the outlet of the solar air heater are presented. The higher outlet temperature of the solar air heater indicates good convective heat transfer.

2. Materials and Methods

2.1. Materials Used for Construction. Plywood: a plywood of 18 mm thickness was used for the construction of the walls of both solar air heaters, which was painted black. The wall was constructed from plywood because it is easily available in Ethiopia, that is, it can be obtained at a low cost. It is also strong enough to support heavy loads. It is light in weight and can be purchased from a local store. The assembly of the solar air heater is done using wood fix, cola, and a glue gun, as shown in Figure 1. For a tight connection with the solar air heater box, the plywood was cut with an L-shaped edge. Cover glass: a simple transparent window glass with a thickness of 4 mm was used at the top of each solar air heater as glazing. An absorber plate, a 1 mm thick black jet coloured painted aluminium sheet, was used. Each absorber plate was painted with black jet paint, and the wall of the solar air heater was painted with black Nifas Kelem. Inlet fan: the solar dryer system is a forced solar dryer. Due to this, there is an inlet computer cooling fan for each solar air heater to force the ambient air to pass through the absorber plate. A computer cooling fan of DC 12V 0.24A Foxconn brushless fan model PVA092G12M is used to force the air to pass over the absorber plate. There is an axial fan at the inlet of each solar air heater. Fans were powered by utility electricity. The materials used in the construction of solar air heaters are presented in Table 1.

2.2. Thermal Performance Analysis. Experiments and measurements are carried out at the same time under the same environment circumstances to achieve precise findings for comparing the performances of the four solar air heaters [26]. The outlet air temperature of two solar air collectors was measured to compare the two solar air collectors [27]. In this study, the outlet temperature was measured to compare the performance of four solar air collectors. A solar air collector having the highest outlet temperature was selected. Additionally, the distribution of the air inside the solar air collector using CFD analysis is also used as an additional comparison [28–33]. Using the outlet temperature of each solar air heater and the results of CFD simulations, the

Figure 1: An experimental setup that shows the south face orientation of four active solar air heaters.

Table 1: Main parts and materials used in the solar air heater constructions.

Parts of solar air heater	Materials used
Wall of the solar air heater	Plywood with thickness of 18 mm, which was painted black
Absorber plate	Aluminium sheet metal with 1 mm thickness which was painted with black jet colour
Glazing	A simple window glass with 4 mm thickness

influence of inlet and outlet positions on the solar air heater due to convective heat transfer was investigated for the performance of each solar air heater.

Percentage increase between each solar air heater is given as follows:

$$P(\%) = \left(\frac{\left(T_{m,i} - T_i\right)}{T_i}\right) \times 100, \quad (1)$$

where "P" denotes the increase in percentage of the solar air heater's average outlet temperature and ambient air temperature above the solar air heater's maximum average outlet temperature. "$T_{m,i}$" is the solar air heater's maximum average outlet temperature, "T_i" is the average temperature of the solar air heater and ambient air, and i is the ambient and solar air heater's number, $i = 0$ for ambient, $i = 1$ for SAH A, $i = 2$ for SAH B, $i = 3$ for SAH C, and $i = 4$ for SAH D. The maximum outlet air temperature is used as a reference to determine the percentage increase of the solar air heater.

2.3. Uncertainty Analysis. The air temperature was measured in this experimental test. There are errors and uncertainties due to the design of the experiments, inaccurate reading of instruments, calibration, and instrument resolution. The overall uncertainty of a measurement is the root-sum-square combination of the uncertainties of all the subordinate measurements considered to be part of the present measurement. This is the uncertainty due to errors introduced by changing environmental conditions such as temperature. For further total uncertainty analysis of the instrument used to measure temperature, sum the square of the uncertainty of the instrument, connection, reading, and other of the instrument itself is calculated and the square root of the summation is obtained [15, 34].

$$U_{\mathrm{OA}} = \sqrt{U_{\mathrm{BE}}^2 + U_{\mathrm{RE}}^2 + U_{\mathrm{OE}}^2 + U_{\mathrm{EE}}^2}. \quad (2)$$

Uncertainty due to repeatability or random error (U_{RE}) is determined from the standard deviation of the sample data.

$$\sigma = U_{\mathrm{RE}} = \sqrt{\frac{\sum_{I=1}^{N}\left(x_i - \overline{x}\right)^2}{N-1}}, \tag{3}$$

where σ is standard deviations, N is number of data measurements, and $\overline{x}$ is the average of the measurements.

The uncertainty due to systematic error for uniformly distributed error (U_{BE}) is given by equation (4):

$$U_{\mathrm{BE}} = \frac{L}{\sqrt{3}}, \tag{4}$$

where $\pm L$ denotes the containment limits which may be taken from manufacturer tolerance. Table 2 shows the manufacturing tolerance limit value of the instrument used in exterminations to measure the temperature. The different uncertainty measurements in the experiment are presented in Table 3.

The result obtained in the uncertainty analysis indicates that the measured data are accurate enough to assess the performance of the designed active solar dryer.

The uncertainty of the solar air heater was calculated using the overall uncertainty of the instrument and the error due to standard deviations and using the equation (2).

The properties of the air were as follows: thermal conductivity of 0.02588 W/m.K, density of 1.164 kg/m^3, specific heat capacity of 1007 J/kg.K, and dynamic viscosity of 1.878×10^{-5}kg/m.s [35].

$$R_e = \frac{\rho \times V \times D}{\mu}, \tag{5}$$

where R_e is Reynolds number; ρ is density, V inlet velocity, D inlet diameter, and μ is dynamic viscosity. By substituting all the known parameters, the Reynold number becomes greater than 2300, which means the flow is turbulent flow [36].

2.4. The Various Types of Solar Air Heaters Studied. The schematic figures of the four different types of solar air heaters with different positions of inlet and outlet in this paper are presented in Figure 2. Solar air heater A (centre to centre), where both the inlet and outlet are at the centre. Solar air heater B (opposite side and corner to corner); both the inlet and outlet of the air are in the opposite corner. Solar air heater C (centre to corner), with the inlet at the centre and the outlet at the corner. Solar heater D (corner to centre) with an inlet at the corner and an outlet at the centre. The centre and corner mean one-half and one-fourth of the width of the solar air heater, respectively. Based on the air movement of active and passive solar air heaters, the difference between the active and passive solar air heaters was also investigated.

2.5. CFD Analysis. For predicting air velocity and temperature, computational fluid dynamics (CFD) has been widely used [30]. Modelling and simulation tools are now critical for constructing efficient solar dryers as well as analysing and predicting the performance of various types of sun drying systems [37]. Ansys Fluent software was used to investigate the thermal behaviour of the solar air collector [27]. The results were compared with the experimental results. Because of its capacity to solve equations for the conservation of mass, momentum, and energy using numerical methods to forecast temperature, velocity profiles, and pressure profiles, computational fluid dynamics (CFD) is widely employed [38]. To solve the governing equations, initial and boundary conditions must be defined around the boundary of the system (domain). Fluent is used since the equations are highly nonlinear and not solvable by explicit, closed-form analytical methods [30]. The CFD analysis is based on the uniformity of air flow distribution.

Because of the increased Reynolds number (Re > 2000) obtained in various conditions, turbulent models were examined in a CFD simulation and the best model was selected. The effects of fluid viscosity, buoyancy, and turbulence must be considered in the modelling process to generate a complete and accurate picture of air distribution and heat transfer through the drying system [32]. The use of CFD simulation software to analyse air flow and temperature changes could be beneficial. A steady heat flow is given as the heating surface's boundary condition. In the model, there is no internal heat source and the temperature and air flow rate at the entrance are both constant [39].

The solver setting employs the semi-implicit method for pressure-linked equations (SIMPLE) scheme, which connects pressure and velocity corrections to apply mass conservation and obtain a pressure field [40]. A double precision solver and tetrahedral cells are included in each sketch. The situation was modelled as a steady-state condition, and the

Table 2: Instruments' manufacturing tolerance limit value.

Parameter	Instrument	Brand and model	Accuracy
Temperature	DHT-22	Thermistor	±0.5°C

Table 3: The uncertainty measured in the experiment.

Parameter measured	Unit	U_{BE}	U_{RE}	U_{OE}	U_{EE}	U_{OA}
Air temperature	°C	±0.289	±0.36	±0	±0	±0.462

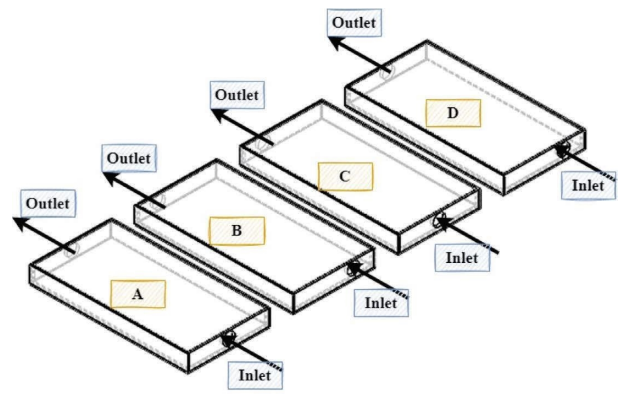

Figure 2: Schematic view of the four SAHs at different positions of inlet and outlet.

best drying chamber design with the most uniform air temperature and air flow distribution was chosen. To verify the CFD simulation results, the optimum design was built and tested under various operating conditions of air flow, temperature, and various geometries of the drying cabinet [30].

The RNG $k-\varepsilon$ model was chosen as the best model for the simulation of solar air heaters after a thorough evaluation of numerous turbulence models that might be used for numerical analysis of solar air heaters. As a result, this study employs the RNG $k-\varepsilon$ model [40]. Among turbulent models, the conventional $k-\varepsilon$ model is still the industry standard, and its successful applications have been recorded in recent literature. The standard $k-\varepsilon$ model is a semiempirical model based on the model transport equations, where k stands for turbulent kinetic energy and ε denotes dissipation rate. The transport equation is derived from the exact equation, but the transport equation for k is derived from physical reasoning and has little resemblance to its mathematically precise counterpart. The detail equations for calculating the turbulent kinetic energy, k and its rate of dissipation, ε, are given in the work of Amanlou and Zomorodian, 2010 [30] and Misha et al., 2013 [38].

The thermodynamic properties of material for glass were taken as the specific heat capacity of 800 J/kg.k, density of 2500 kg/m^3, emissivity of 0.925, refractive index of 1.5, and thermal conductivity of 0.7 w/mk [40]. For aluminium and wood, thermodynamic properties specified in the Ansys Fluent Material Library, similar to the thermophysical properties of air, were taken by default from the Ansys Fluent Material Library.

The quality of the grid was determined by confirming that the skewness and orthogonal quality of all pieces were within acceptable bounds (less than 0.95 and greater than 0.15, respectively) [41]. A skewness of 0.48 was determined on this basis. The mesh skewness of the cabinet was also assessed throughout the simulation. For the fine mesh, it was less than 0.48, which is suitable for CFD simulation [32].

In this investigation, the set value for convergence was 10^{-4}, and when it fell below that, the solving process came to a halt. Correct convergence findings and iteration were used to map the airflow distribution and heat transfer inside the solar air collector [32]. The simulations were run using Fluent's pressure-based model. The scaled residuals' convergence requirements for the continuity and momentum equations were set to 10^{-4}, and for the energy equation and mesh metric skewness, they were set to 10^{-5} [32]. The residual value is a convergence statistic that determines when a solution has reached a point of convergence. The three key boundary conditions investigated were the steady-state condition, the energy equation, and the $k-\varepsilon$ of the viscous model, with a convergent value of 10^{-4} [32]. The number of tetrahedral cells, number of nodes, maximum minimum average, and standard deviations of mesh metrics for four different solar air heaters are presented in Table 4.

2.6. Experimental Investigations. The experiment was carried out at Addis Ababa Science and Technology University (AASTU) in Addis Ababa, Ethiopia, close to the College of Electrical and Mechanical Engineering (CEME). It is at a latitude of 8.88327 and a longitude of 38.810327 degrees. The study of the effect of the positions of the inlet and outlet was conducted after the calibration of both the sensor, the solar air heater at similar conditions and knowing the orientation of the proper solar air heater. The experiment was done from 9: 00 AM to 5: 00 PM between February 24, 2022, and March 02, 2022, to study the position of the inlet and outlet of the solar air collector and between May 24 and 26, 2022, for identification of the proper face orientations. A time interval of between 15 and 20 minutes was used for recording the data. Four similar solar air heaters with different positions of inlet and outlet (Solar Air Heaters A, B, C, and D) were considered in this study. The heater was constructed using the ratio of length to width of two, or with internal dimensions of 1 m in length and 0.5 m in width and a depth of 9 cm. Each solar air heater was constructed from similar materials. All outside walls of the solar air heater except the cover glass were painted black to decrease the loss of temperature by increasing the outside temperature near the solar air heater. The diameter of the inlet and outlet was 7.5 cm for the active solar air heater. For the passive solar air heater, the inlet area is equal to the internal cross-sectional area of the solar air heater, which is at the width of 50 cm and the depth of 9 cm of the solar air heater and outlet of 7.5 cm. The tilt angle was zero, or horizontal, 5.74 and 12 degrees inclined. The solar air heater was designed for 1.5 kg of banana with an initial and final moisture content of 80% and 15%, respectively, and a drying air outlet temperature of 50°C. The other design parameters of temperature, relative humidity, solar radiation, and others were taken from the National Metrology Agency of Ethiopia, Addis Ababa, and NASA. The 3D modelling of the solar air heater was done using solid work and the file is saved in IGES format for inserting the geometry into Ansys Fluid Fluent. The outlet temperature of each solar air heater and the ambient air temperature were measured and recorded.

2.7. Experimental Procedure. First, the measuring instrument was calibrated under similar weather conditions by taking a total of 54 measurements. Then, the test of each solar air heater at similar conditions, having a corner inlet and centre outlet, was carried out on two different days at different tilt angles of 5.74° and 12°. A total of 35 data for each solar air heater was taken. For the investigation of the south face orientation of the solar air heater, four similar air collectors having an angle of 15 degrees between each solar air heater were used to know the exact south position from the horizontal centroid line as shown in Figure 1. The investigations into the effects of the positions of the inlet and outlet were done after removing the previous inlet and outlet. For the effect of the positions of the inlet and outlet, the experimental test was carried out on three different days at different tilt angles of horizontal, or zero°, 5.74°, and 12°. Figure 3 shows the experimental study of the positions of the

Table 4: The number of tetrahedral cells for four different solar air heaters.

Sketch	Tetrahedral cell	Number of nodes	Mesh metric			
			Min	Max	Aver	SD
SAH A	1975134	373215	$1.3643e-004$	0.69559	0.24006	0.10865
SAH B	1976653	373421	$2.6557e-004$	0.63113	0.23992	0.1087
SAH C	1976408	373393	$2.6945e-004$	0.60009	0.23992	0.10847
SAH D	1977148	373482	$2.9713e-004$	0.61734	0.2398	0.10855

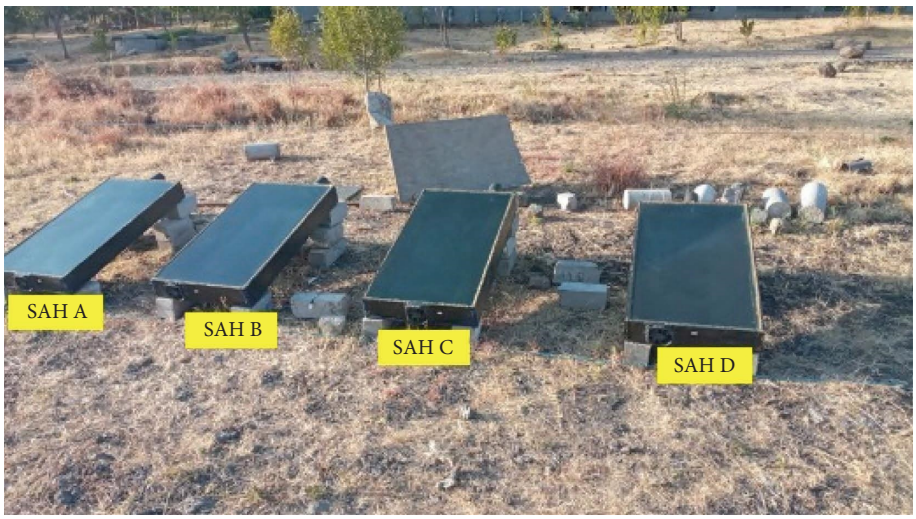

Figure 3: Experimental setup of four active solar air heaters at different positions of the inlet and outlet.

inlet and outlet at 12°. After all was done, the performance test for active and passive solar air heaters was carried out for two days at two different tilt angles of zero or horizontal, 5.74 and 12°.

From Figure 3, A is centre to centre, B is corner to corner, C is centre to corner, and D is corner to centre (corner means one-fourth, and the centre is one-half of the width of the solar air heater). The four solar air heaters are placed in some orientations and tilt angles, but the installation of the fan and the exit of the air are different for each solar air heater. The effect of the forced convective heat transfer at different positions of the inlet and outlet was evaluated based on the experimental setup shown in Figure 3.

Figure 4 represents the experimental setup of active and passive solar air heaters. The south face of the solar air collector for solar radiation and wind flow direction and the positions of the outlets for active and passive solar air collectors are similar, with a similar south face and tilt angle. In the active solar air heater, there is a computer cooling fan at the inlet, and in the passive solar air heater, it is open, so the cross-section area of the inlet is equal to the cross-sectional area of the solar air heater.

2.7.1. Experimental Investigation on Solar Air Collector Face Identifications. The south and north faces of the solar air collector were identified using two similar active solar air collectors. The outlet temperature of each solar air collector is measured to identify the proper face orientation. In this experimental investigation, the calibrations for the measuring devices, solar air collector one and two, at similar conditions were carried out. The experimental setup in Figures 5(a) and 5(b) represents calibrations and proper face orientations of the two solar air collectors on May at tilt angle of latitude minus 25 degree as presented on the literature [42] for latitude of between 1 and 14 degree.

3. Results and Discussion

The setup section was carried out using double precision and serial. The solver is pressure-based, absolute velocity formulation, steady, and gravity-based. Inlet: the mass flow rate is 0.0101 kg/s with a 75 mm diameter. That is a velocity of 2m/s. Outlet: assuming the gauge pressure is zero. Wall: the side wall of the collector is assumed with no heat loss. Even though the simulation was carried out in three dimensions, the analysis was carried out on the symmetry plane [38]. The state is steady and the absorber is at a constant temperature of 126.85°C.

3.1. CFD Simulation Result. The CFD simulation results for temperature, velocity vector, velocity profile, and streamline are presented for four different arrangements of solar air heaters. Data analysis of the four proposed plans was carried out using CFD to determine the suitability of the design of the new solar air heater. By analysing the uniformity of airflow distribution in the solar air collector, the most practicable design may be

Figure 4: Experimental setup for active and passive solar air heaters.

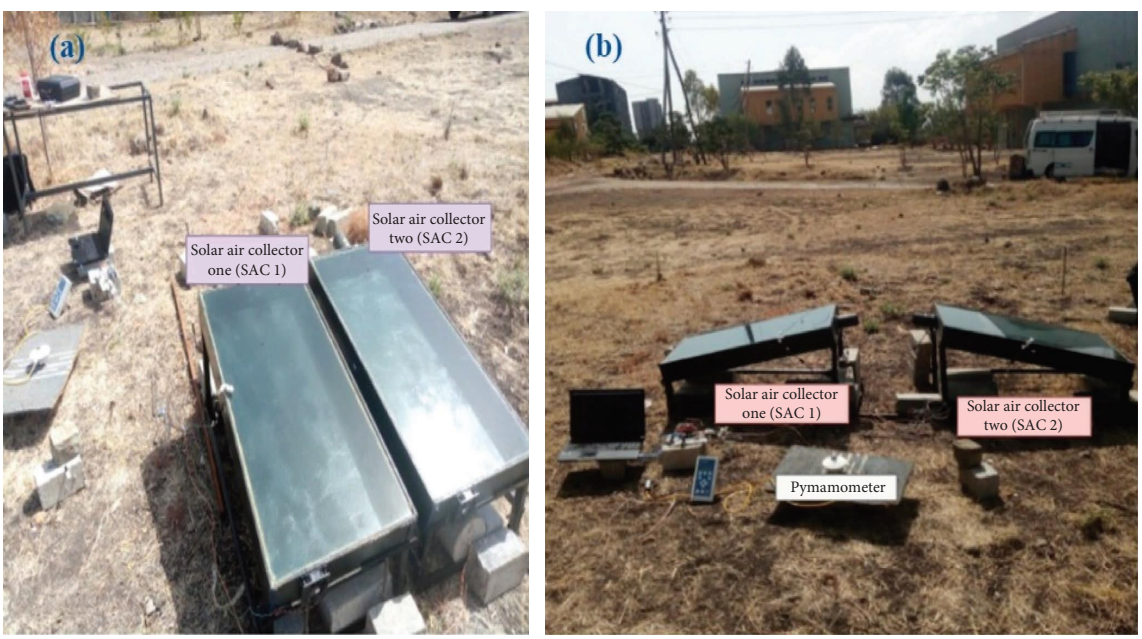

Figure 5: Experimental setup for the calibrations (a) and face identification (b).

determined [30]. The temperature and airflow distributions of the solar air heater may be predicted using the 3D CFD model. The effect of the positions of the forced convective heat transfer at different positions of the inlet and exit of the solar air collector using 3D solar air heater symmetry was investigated in Figure 6 and Figure 7. The temperature contour shown in Figure 6, velocity contour, and stream line were presented using the CFD simulation result as shown in Figure 7.

In comparison with the others, the temperature profile at SAH B is the best in Figure 6. When compared to other solar air heaters, the air movement is not as straightforward. Due to good convective heat transfer, the time spent by the air on the absorber plate contact increases when there is a bending

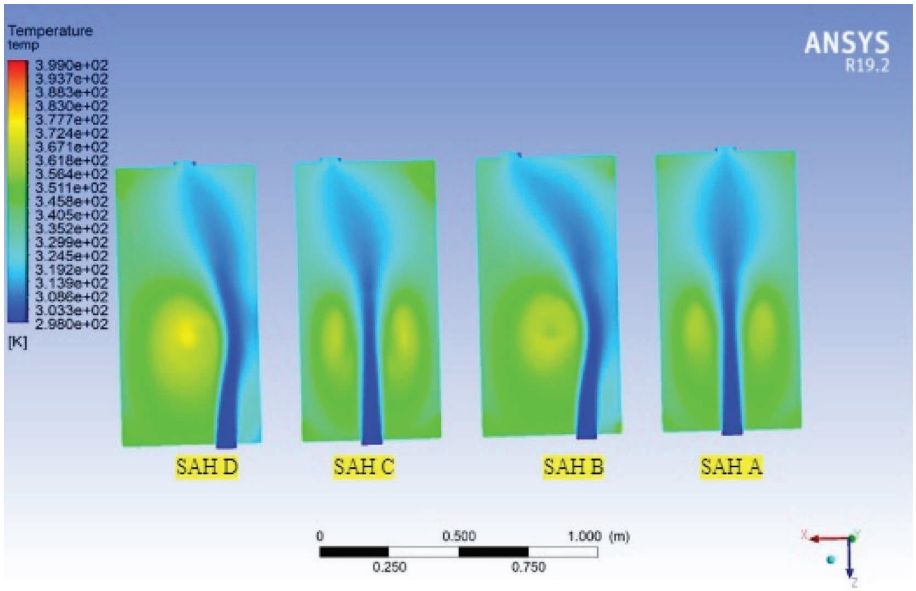

Figure 6: Air temperature distributions for the four solar air collector design CFD simulation results at constant temperature of the absorber at 126.85°C and inlet temperature of 25.05°C.

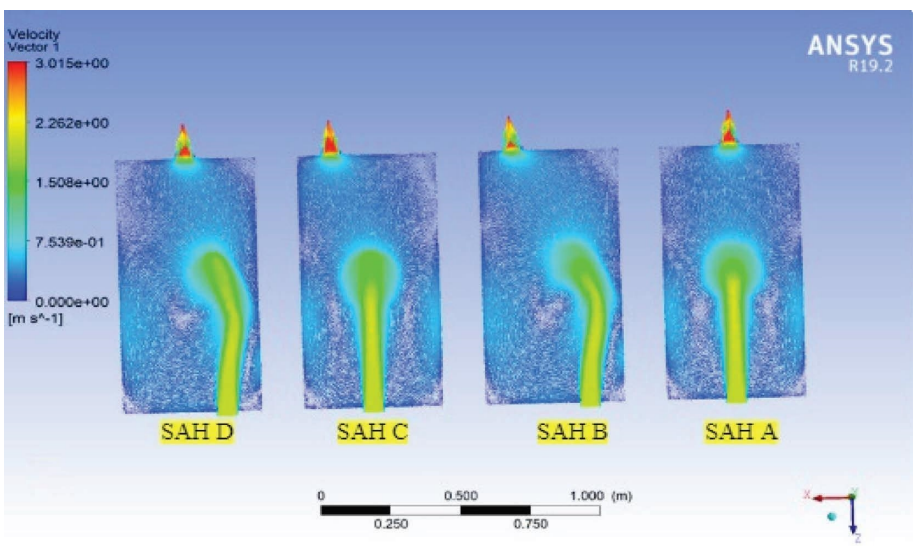

(a)

Figure 7: Continued.

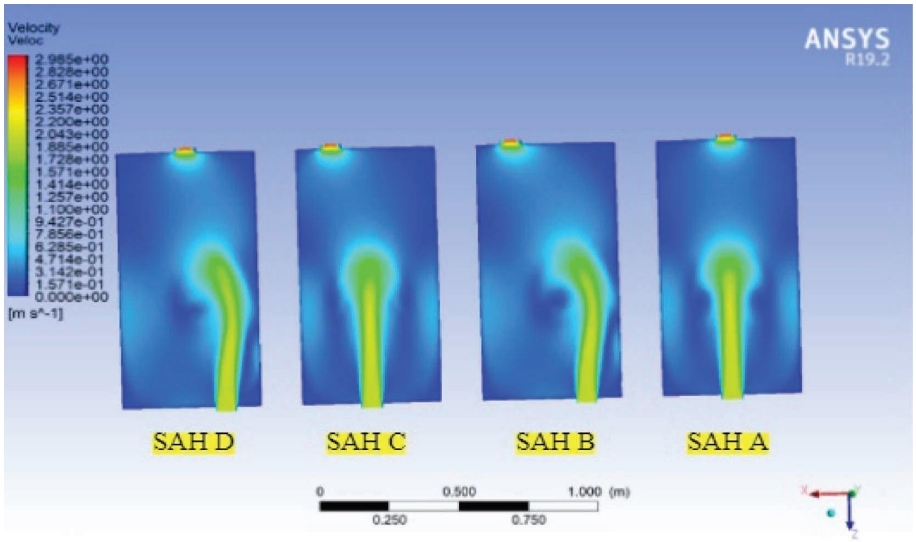

(b)

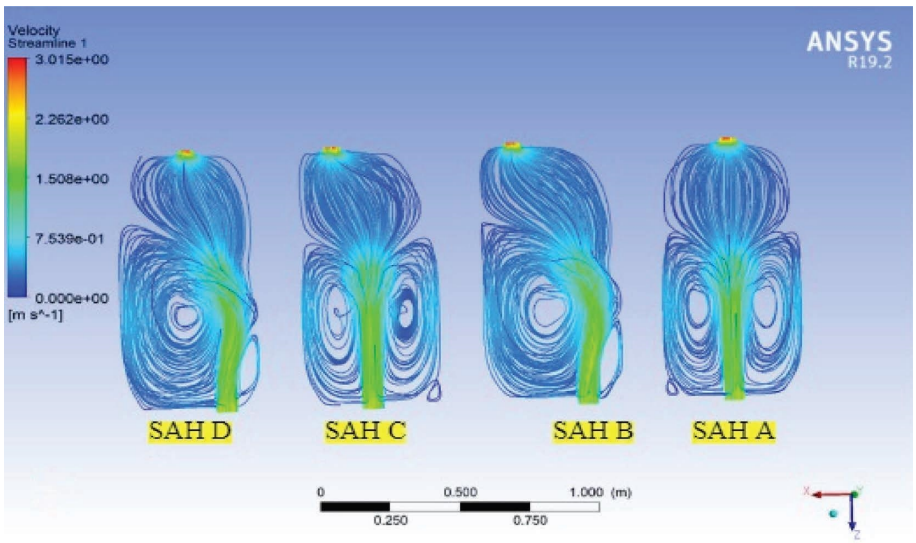

(c)

Figure 7: Air velocity distributions of vector (a), contour (b), and streamline (c) profiles for the four solar air heaters at an inlet velocity of 2 m/s.

flow, and the air gains more energy than in other cases. The temperature in the symmetry plane of the solar air heater is shown in the CFD simulation in Figure 6. In the case of SAH B, when air travels through the absorber plate, the temperature rises in the shortest time and distance from the inlet when compared to others.

Figure 7 presents the velocity vector, contour, and stream lines of the air at the symmetry plane of four different solar air heaters due to convective heat transfer. As shown in Figure 7(a), the velocity vector has a good air distribution in the symmetry plane in the case of SAH B. There is a bent flow in solar air heaters B and D, but there is a difference near the outlet of the solar air heater. In the case of SAH B, there is a good flow of air. In the case of SAH A and SAH C, the flow is straight forward at the initial and it starts to distribute. When compared near to the outlet, there is the best flow configuration in SAH C. The air inlet and outlet are inline in SAH A, and the air flows directly through the outlet. The time spent on contact between the air and the absorber plate is short in comparison to the other two cases, resulting in poor convective heat transfer in SAH A. The results of the CFD simulation and the results of the experiential tests agree very well. During the experiment, the outlet air temperature was lowest in the case of solar air heater A, that is, SAH A, since the outlet temperature was the smallest in the case of solar air heater A, SAH A.

The hot air distribution was not improved by shifting the inlet and outlet of solar air heaters C and D. The difference between solar air heaters C and D is that the solar air heater's inlet and outlet are different. The distinction between solar air heaters C and D is that the inlet for solar air heater C becomes the outlet for solar air heater D, and vice versa.

When the air enters the corner inlet of the solar air heater, the flow is not straight and forward; there is a bend. This increases the time of the air on the solar air heater, which increases the outlet temperature.

According to the CFD simulation, solar air heater B has the optimum air temperature and air flow distribution, making it the optimal design for various applications such as air heating and drying. When a separate drying chamber is linked to the solar air heater, the solar air heater D is the optimal choice because it is directly connected to the drying chamber via a duct, resulting in minimal pressure drop and optimal performance. During the experimental performance test, the solar air heater SAH B gave the best outlet temperature compared to others.

A more uniform air velocity distribution is achieved by moving the exit from the centre to the left or right corner, and the inlet to the right or left corner, respectively. The velocity will weaken the temperature distribution when the intake and outflow positions are in line as shown in Figure 6, SAH A and SAH. Although the design of solar air heater B appears to be the best, it is not suggested for solar dryers because the outlet is not in the middle, making it difficult to supply the drying chamber in the case of a single solar air heater. In the case of a solar air heater, it is possible to use the inlet corner and outlet corner. In this scenario, it is preferable to use the intake at the corner and the exit in the middle for an indirect active solar dryer. In this investigation, the difference between using the intake at the corner and the exit at the centre is only 25%, since the width of the solar air heater is 50 cm. The effect of shifting the exit of the direct hot air supply to the drying chamber is proportional to the fraction of the width taken for the input and outlet positions. In Figures 7(a)–7(c), the air spent more time inside the solar air heater that means it can get much energy.

As shown in Figure 7 of the stream line, in a solar air heater A, the air flows in a straight line because the positions of the inlet and outlet are in the same line. Due to that, the air entering the solar air heater leaves the solar air heater without spending more time inside the solar air heater. As a result, the outlet air temperature and the convective heat transfer rate decrease. Since the heat energy due to convective heat transfer is directly related to the change in temperature of the outlet and inlet. In SAH B, the air spends more time inside the solar air heater, which increases the heat gain of the air inside the solar air heater, and the outlet temperature increases.

3.2. Experimental Testing. In the calibration of each temperature sensor, a total of 54 measurements were taken and the uncertainty fell between 0.041 and 0.384, which is the acceptable range used by different researchers for temperature sensors. For solar air heaters, a total of 35 data points were collected, with the uncertainty ranging from 0.14 to 0.23 for each solar air heater.

3.2.1. Experimental Investigation on Solar Air Collector. The uncertainty analysis of the instruments and solar air heater was carried out and was found to be in the range of 0.041 to 0.384 and 0.14 to 0.23, respectively.

(1) Solar Air Heater with Similar Inlet and Outlet Positions. Each heater produces almost comparable quantities of output air temperature due to similar conditions. During the experiment test, the uncertainty for SAC 1, SAC 2, SAC 3, and SAC 4 at different tilt angles is nearly negligible for similar solar air collectors from the corner entry to the centre exit, as illustrated in Figure 7. This suggests that the solar heaters are performing similarly. Each solar air collector's average exit temperatures are approximately equal at similar conditions.

The outlet temperatures of the four comparable solar air collectors are shown in Figure 8, together with the ambient air temperature, which is used to determine the uncertainty of the solar air collector. The speed of the wind causes the ambient air temperature to fluctuate. The temperature near the sensor drops when there is wind, and vice versa.

(2) Solar Air Collector at Different South Face Orientations. As shown in Figure 1, there are four solar air collectors at different orientations (O). The angle between the consecutive solar air collectors was 15 degrees. The outlet temperature of the solar air collector at different orientations of SAC orientation 1 (TO-1, out), SAC orientation 2 (TO-2, out), SAC orientation 3 (TO-3, out), SAC orientation 4 (TO-4, out), and the ambient air temperature (Tamb) versus time is plotted in Figure 2.

There is no significant difference when the average outlet temperature of each solar air heater is measured in Figure 8. As shown by the average outlet temperature of different orientations of solar air heaters in Figure 9, the solar air heater of O-3 is 0.68%, 0.59%, and 0.63% higher than the solar air heaters' orientations of O-1, O-2, and O-4, respectively. This indicates that there is no significant change in the temperature of each solar air heater orientation during the south face between February 27 and 28, 2022. For the northern hemisphere, there is a recommendation to use south face orientations for annual optimum tilt angle, but it is better to check even the south face orientations with some angle greater than 15 degrees between the consecutive solar air collectors to know the proper south face orientations.

(3) Solar Air Heater at Different Positions of Inlet and Outlet. The temperature of the solar air collector's outflow begins to rise in the morning and reaches its peak about midday. It begins to fall in the afternoon. The graph represents the ambient air temperature and the outlet temperature of four solar air collectors at different positions of inlet and outlet (T SAC A, out; T SAC B, out; T SAC C, out; T SAC D, out).

From Figure 10, the temperature of the solar air collector B is greater than the temperature of the other solar air collector all day. This implies the solar air collector B has a higher outlet temperature. A maximum outlet temperature was obtained at mid-day.

As presented in Table 5, based on the three-day average outlet temperature of solar air heaters at different tilt angles, the solar air heaters A, B, C, and D provide 24.99, 33.83, 25.70, and 28.45 percent more than the ambient air's three days average temperature. Based on the three-day average outlet temperature of solar air heaters at different tilt angles,

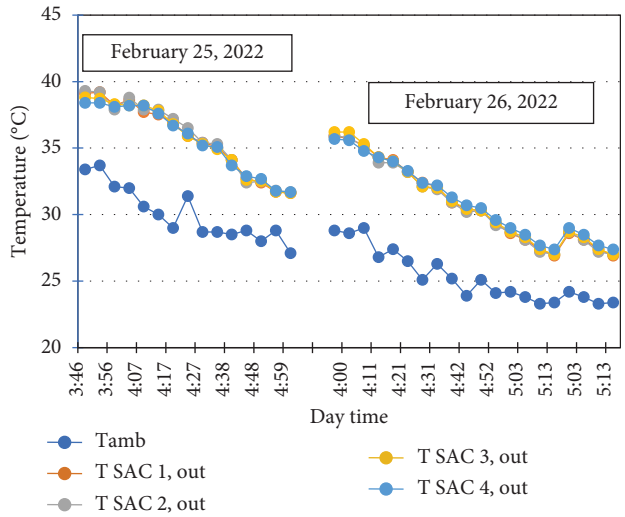

Figure 8: Ambient and outlet temperature profiles of each SAC on February 25 and 26, 2022.

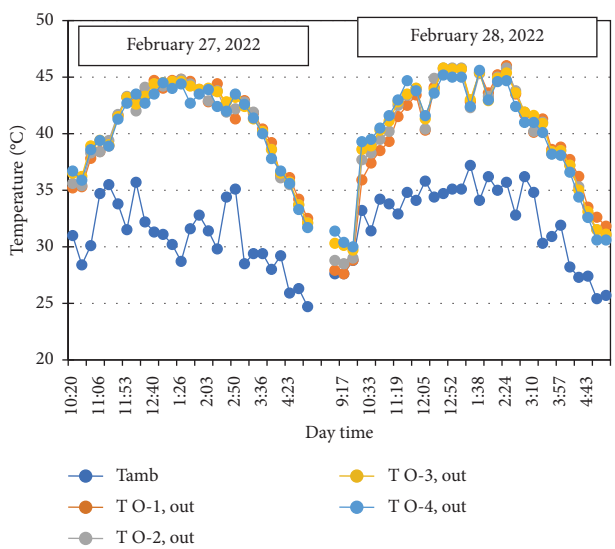

Figure 9: The outlet temperature versus drying at different face orientations.

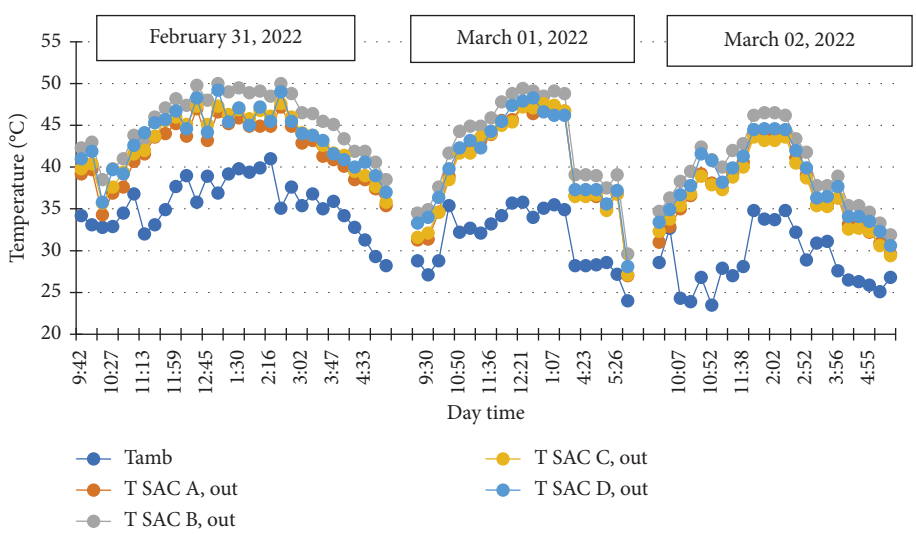

Figure 10: The outlet temperature versus drying time of four different solar air collectors.

Table 5: Ambient and average outlet temperatures of the solar air collector.

Day	Ambient and outlet average temperatures of the solar air collector				
	Tamb	SAC A, out	SAC B, out	SAC C, out	SAC D, out
Day-1 February 31, 022 (0°)	35.45	41.98	45.39	42.92	43.44
Day-2 March 01, 022 (5.74°)	31.43	40.12	42.55	40.12	40.79
Day-3 March 02, 2022 (12°)	28.75	37.06	39.68	36.90	38.25
Average	31.88	39.72	42.54	39.98	40.82

a solar air heater B provides 33.46, 7.11, 6.40, and 4.20 percent more than the ambient three-day average outlet temperature of solar air heaters A, C, and D, respectively. From the experimental result of three days with three different tilt angles, the average outlet temperature of solar air collectors A, B, C, and D, with various inlet and outlet positions and tilt angles, is 39.72°C, 42.54°C, 39.98°C, and 40.82°C, respectively, compared with the average temperature of ambient solar air collector B, which gives 10°C more.

(4) The Effect of the Tilt Angle on the Average Outlet Temperature. A minimum average outlet temperature was obtained in solar air collectors A and C when compared to solar air collectors B and D at different tilt angles all day.

The average outlet temperature of four solar air heaters at three different tilt angles is shown in Figure 11. At various tilt angles, this is the temperature difference between the average outlet air temperature of each solar air collector and the ambient air temperature. Day one is February 31, 2022; day two is March 1, 2022; and day three is also March 2, 2022. The percentage change in temperature of the solar air collector outlet and the average ambient temperature increase as the tilt angle increases, as indicated in Figure 11. When compared to a tilt angle of 0 degrees, the percentage change is the largest at 12 degrees, but there is no more significant difference when compared to a tilt angle of 5.74 degrees. The change in temperature increases rapidly from tilt angle 0 to 5.74, but there is no more substantial change in exit temperature at tilt angle 12 compared to the 5.74 tilt angle. Next to the solar air collector B, solar air collector D delivers the optimum outlet temperature based on the percentage increment of the outlet average air temperature.

(5) Active and Passive Solar Air Collector. According to Figure 12, the average outlet temperature of the passive solar air collector is 17% and 4.43% higher than the ambient and active solar air collectors, respectively. Due to fluctuations in wind speed, the outlet temperature of the passive solar air collector and the ambient air temperature fluctuate. The higher outlet temperature of the passive solar air collector is higher than that of the active solar air heater due to the air speed.

3.3. Experimental Investigation for Face Orientation of SAC in May. Before the orientation's identification, the two solar air collectors should be calibrated. The uncertainty of the sensor is included during these calibrations at some conditions. During the identification of the uncertainty of the two solar air collectors, it becomes in the range of −0.12448 and + 0.124476 for solar air collectors one and two,

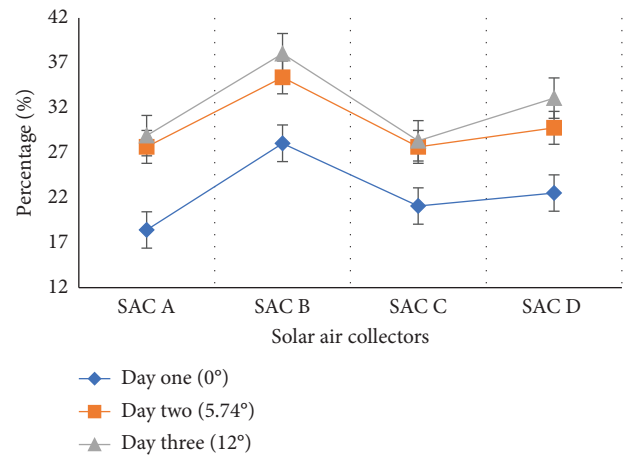

Figure 11: Percentage increase of average outlet temperature at different tilt angles.

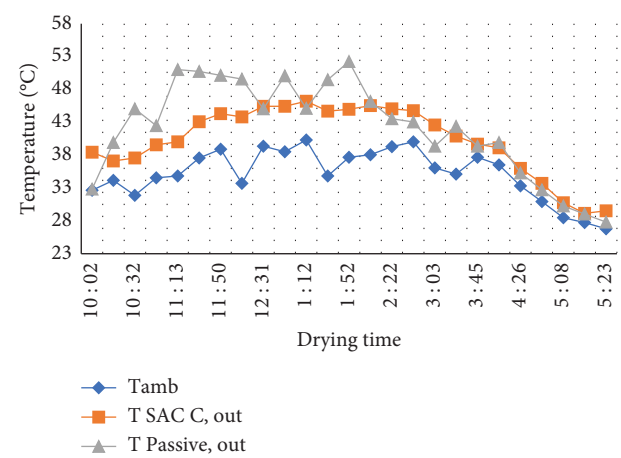

Figure 12: The temperature of active, passive, and ambient air on March 4, 2022.

respectively. Figure 13 represents the outlet temperature and relative humidity of two solar air collectors and the ambient air temperature and relative humidity at similar conditions. SAC 1, T and SAC 1, RH are the outlet temperature and relative humidity of solar air collector one on the south face. SAC 2, T and SAC 2, RH are the outlet temperature and relative humidity of the solar air collector two on the south face. Tamb and RHamb are the temperature and relative humidity of the ambient air.

As shown in Figure 13, the outlet temperature for both solar air collectors one and two is approximately equal at similar conditions.

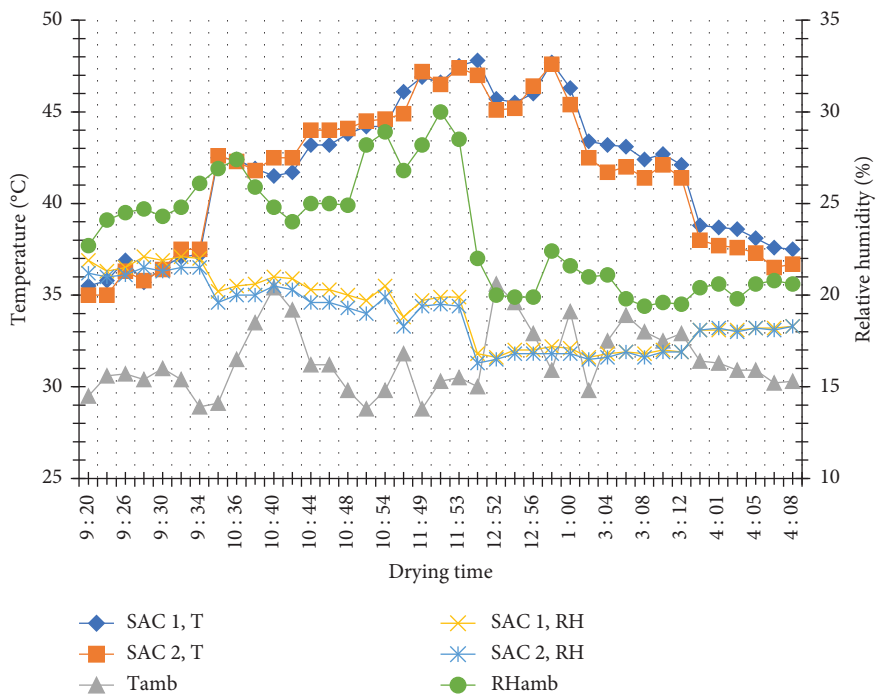

Figure 13: Temperature and relative humidity on May 24, 2022.

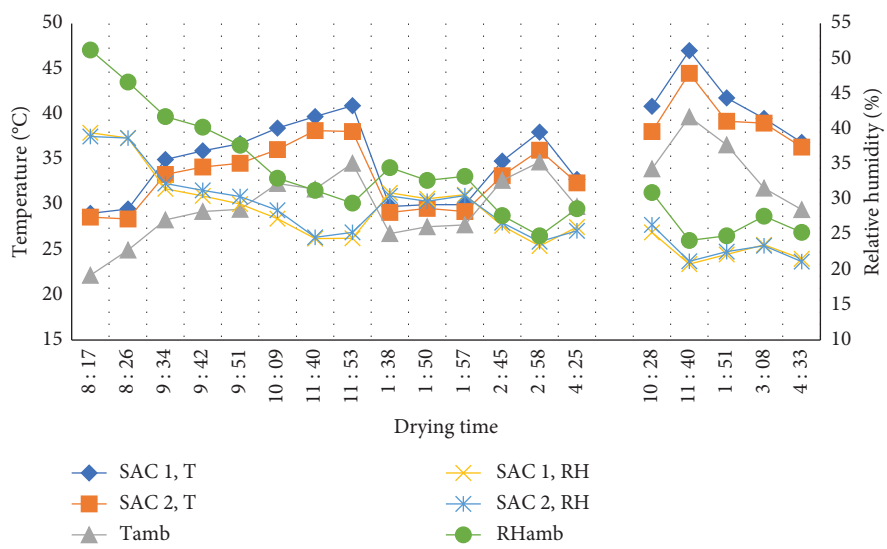

Figure 14: Temperature and relative humidity on May 25, 2022 and May 26, 2022.

3.3.1. Different Face Orientations of Solar Air Collector. For the north and south face orientations with the fan at 12 V on May 25, 2022, the maximum outlet temperatures of 40.15°C and 37.91°C were obtained, respectively, with solar radiation at the time of 11: 49AM. The north face orientations give 1.775°C more than the south face orientations, and when the north and south face orientations' outlet temperatures are compared with the ambient air temperature, there is an increase of 15.61% and 9.68%, respectively. The average outlet temperature of the solar air collector with north-facing orientation is 5.23% higher than the solar air collector with south-facing orientation.

When the voltage of the fan becomes 9 V on May 26, 2022, the average outlet temperature of the solar air collector in the north face orientation is 5.07% more than the solar air collector in the south face orientation. The average outlet temperature of the two solar air collectors in the north and south face orientations is 19.38% and 13.62% more than the ambient air temperature.

The outlet temperature of the two solar air collectors increases when the voltage of the fan decreases from 12 V to 9 V. When the voltage decreases, the speed of the air decreases as well. Due to this, the solar air collector outlet temperature increases. The negative tilt angle based on

literature indicates the north face orientation for latitudes of between 1 and 14 degrees. When the average outlet temperature was measured, the north-facing orientation gave better results than the south-facing orientation. At a solar radiation of 929.69 w/m^2 on the day of May 26, 2022, at 11: 40AM, the outlet temperature of the solar air collector on the north and south faces became 47.03 and 44°C, respectively, at 9 V.

The outlet temperature and relative humidity versus drying time of the two solar air collectors and the ambient air is shown in Figure 14. SAC 1, T and SAC 1, RH are the outlet temperature and relative humidity of solar air collector one on the south face. SAC 2, T and SAC 2, RH are the outlet temperature and relative humidity of the solar air collector two on the south face. Tamb and RHamb are the temperature and relative humidity of the ambient air. Based on Figure 14, the temperature and relative humidity have inverse relationships. Based on the graph, the solar air collector one (SAC 1) temperature is greater than the SAC temperature. On May 25, 2022, when there is cloud and no sunlight, the outlet temperature of the two solar air collectors and ambient air decreases. On this day, the north face solar air collector also gives good results when compared with the south face solar air collector.

4. Conclusions

The uncertainty analysis of the instruments and solar air heater was carried out and was found ±0.465°C and ±0.462°C, respectively. According to many studies, the true south face is the best orientation for a solar air heater in the northern hemisphere. The average outlet temperature of the solar air heater of O-3 is 0.68%, 0.59%, and 0.63% higher than the solar air heaters' the orientation of O-1, O-2, and O-4, respectively. The average output temperature of the solar air heater rises as the tilt angle of the solar air heater rises. The effect of the tilt angle can be determined by conducting an experiment on various days at various tilt angles and determining the difference in temperature between the average output temperature of the solar air heater and the ambient air temperature on each day. As a result, the output temperature of the forced solar air heater is lower than that of the passive. The average outlet temperature of the passive solar air heater is 17% and 4.43% higher than that of the ambient and active solar air heaters, respectively.

Instead of taking the optimum annual tilt angle as much as possible, it is better to take the optimum seasonal tilt angle, and if possible, it is better to take the monthly tilt angle. The recommended tilt angle for locations with latitudes between 1 and 14 degrees, provided by [42], gives a good outlet temperature.

Based on the investigations, the positions of the inlet and outlet of the solar air heater affect the outlet temperature of the solar air heater. The average outlet temperature of the solar air heater B is higher than the average temperature of the ambient and the average outlet temperatures of solar air heater A, solar air heater C, and solar air heater D by 25.07%, 6.64%, 6.02%, and 4.03%, respectively.

The average outlet temperature of solar air heater B is 10°C higher than the ambient air's average outlet temperature. According to the CFD simulation, solar air heater B has good air temperature and air flow distribution, making it a good design for various applications such as air heating and drying. Based on the three-day average outlet temperature of solar air heaters, the solar air heaters A, B, C, and D provide 24.99, 33.83, 25.70, and 28.45 percent more than the ambient air's three-day average temperature.

Convective heat transfer is the main parameter in the design of the solar air heater and solar drying system. The outlet temperature of the solar air heater with natural convective heat transfer is higher than that of forced convective heat transfer.

Due to the variation in the speed of the wind, there is a fluctuation in the temperature of the ambient air. However, during the forced fixed inlet of the air into the solar air heater, the temperature does not have a great fluctuation. It is near to fixed compared to natural convective heat transfer.

Researchers can verify their findings by repeating the procedure and checking for other fractions of the solar air heater's width. In this study, the proportion considered for the corner inlet or outlet was 25% of the width from the end edge, and for the centre inlet or outlet, it was 50% of the width of the solar air heater.

Data Availability

The data used to support the findings of this study are included within the article.

Conflicts of Interest

The authors declare that there are no conflicts of interest regarding the publication of this paper.

Acknowledgments

I wish to thank the staff of Mechanical Engineering department and the staff of AASTU innovation centre and mechanical machine shop, advisor Samson Mekbib (Assoc. Prof), my family, my beloved and friends, NMA of Ethiopia, and the University of AASTU for helping and allowing me to build the solar air collector, and others who helped me to achieve this success.

References

[1] A. Tiwari, "A review on solar drying of agricultural produce," *Journal of Food Processing and Technology*, vol. 7, no. 9, 2016.

[2] O. Kilanko, T. Ilori, R. Leramo et al., "Design and performance evaluation of a solar dryer," *Journal of Physics: Conference Series*, vol. 1378, no. 3, Article ID 32001, 2019.

[3] M. F. El-khawajah, L. B. Y. Aldabbagh, and F. Egelioglu, "The effect of using transverse fins on a double pass flow solar air heater using wire mesh as an absorber," *Solar Energy*, vol. 85, no. 7, pp. 1479–1487, 2011.

[4] M. E. A. Slimani, M. Amirat, S. Bahria, I. Kurucz, M. Aouli, and R. Sellami, "Study and modeling of energy performance of a hybrid photovoltaic/thermal solar collector: configuration

suitable for an indirect solar dryer," *Energy Conversion and Management*, vol. 125, pp. 209–221, 2016.

[5] J. Assadeg, A. H. A. Al-waeli, A. Fudholi, and K. Sopian, "Energetic and exergetic analysis of a new double pass solar air collector with fins and phase change material," *Solar Energy*, vol. 226, pp. 260–271, 2021.

[6] A. Fudholi and K. Sopian, "A review of solar air flat plate collector for drying application," *Renewable and Sustainable Energy Reviews*, vol. 102, pp. 333–345, 2018.

[7] M. K. Mittal and L. Varshney, "Optimal thermohydraulic performance of a wire mesh packed solar air heater," *Solar Energy*, vol. 80, no. 9, pp. 1112–1120, 2005.

[8] F. Struckmann, "Analysis of a flat-plate solar collector," 2008, https://www.lth.se/fileadmin/ht/Kurser/MVK160/Project_08/Fabio.pdf.

[9] J. O. Almirón and M. A. Lara, "Experimental development of solar collector of unconventional air," *Sustainable Energy*, vol. 4, no. 1, pp. 17–27, 2016.

[10] R. Bakari, "Heat transfer optimization in air flat plate solar collectors integrated with baffles," *Journal of Power and Energy Engineering*, vol. 6, no. 1, pp. 70–84, 2018.

[11] A. A. El-Sebaii and S. M. Shalaby, "Experimental investigation of an indirect-mode forced convection solar dryer for drying thymus and mint," *Energy Conversion and Management*, vol. 74, pp. 109–116, 2013.

[12] M. Kumar, S. K. Sansaniwal, and P. Khatak, "Progress in solar dryers for drying various commodities," *Renewable and Sustainable Energy Reviews*, vol. 55, pp. 346–360, 2016.

[13] O. Ekechukwu and B. Norton, "Review of solar-energy drying systems II: an overview of solar drying technology," *Energy Conversion and Management*, vol. 40, no. 6, pp. 615–655, 1999.

[14] A. El Khadraoui, S. Bouadila, S. Kooli, A. Guizani, and A. Farhat, "Solar air heater with phase change material: an energy analysis and a comparative study," *Applied Thermal Engineering*, vol. 107, pp. 1057–1064, 2016.

[15] E. K. Akpinar and F. Koçyiĝit, "Energy and exergy analysis of a new flat-plate solar air heater having different obstacles on absorber plates," *Applied Energy*, vol. 87, no. 11, pp. 3438–3450, 2010.

[16] R. Poblete, E. Cortes, J. Macchiavello, and J. Bakit, "Factors influencing solar drying performance of the red algae Gracilaria chilensis," *Renewable Energy*, vol. 126, pp. 978–986, 2018.

[17] P. J. Etim, A. B. Eke, and K. J. Simonyan, "Design and development of an active indirect solar dryer for cooking banana," *Scientific African*, vol. 8, Article ID e00463, 2020.

[18] I. C. Macedo and C. A. C. Altemani, "Experimental evaluation of natural convection solar air heaters," *Solar Energy*, vol. 20, no. 5, pp. 367–369, 1978.

[19] R. Bakari, R. J. A. Minja, and K. N. Njau, "Effect of glass thickness on performance of flat plate solar collectors for fruits drying," *Journal of Energy*, vol. 2014, Article ID 247287, pp. 1–8, 2014.

[20] H. S. Dheyab, M. S. M. Al-Jethelah, T. A. Yassen, and T. K. Ibrahim, "Experimental study of the optimum air gap of a rectangular solar air heater," *Journal of Advanced Research in Fluid Mechanics and Thermal Sciences*, vol. 59, no. 2, pp. 318–329, 2019.

[21] A. O. Dissa, J. Bathiebo, S. Kam, P. W. Savadogo, H. Desmorieux, and J. Koulidiati, "Modelling and experimental validation of thin layer indirect solar drying of mango slices," *Renewable Energy*, vol. 34, no. 4, pp. 1000–1008, 2009.

[22] V. Gupta, L. Sunil, A. Sharma, and N. Sharma, "Construction and performance analysis of an indirect solar dryer integrated with solar air heater," *Procedia Engineering*, vol. 38, pp. 3260–3269, 2012.

[23] J. Banout, J. Havlik, M. Kulik, P. Kloucek, B. Lojka, and I. Valterova, "Effect of solar drying on the composition of essential oil of sacha culantro (eryngium foetidum l.) grown in the peruvian amazon," *Journal of Food Process Engineering*, vol. 33, no. 1, pp. 83–103, 2008.

[24] J. P. Ekka, K. Bala, P. Muthukumar, and D. K. Kanaujiya, "Performance analysis of a forced convection mixed mode horizontal solar cabinet dryer for drying of black ginger (Kaempferia parviflora) using two successive air mass flow rates," *Renewable Energy*, vol. 152, pp. 55–66, 2020.

[25] K. R. Arun, G. Kunal, M. Srinivas, C. S. S. Kumar, M. Mohanraj, and S. Jayaraj, "Drying of untreated Musa nendra and Momordica charantia in a forced convection solar cabinet dryer with thermal storage," *Energy*, vol. 192, Article ID 116697, 2020.

[26] M. Al-neama and I. Farkas, "Utilization of solar air collectors for product's drying processes maytham," *Journal of Scientific and Engineering Research*, vol. 5, no. 2, pp. 40–56, 2018.

[27] H. Ö. Güler, A. Sözen, A. D. Tuncer et al., "Experimental and CFD survey of indirect solar dryer modified with low-cost iron mesh," *Solar Energy*, vol. 197, pp. 371–384, 2020.

[28] S. Sonthikun, P. Chairat, K. Fardsin, P. Kirirat, A. Kumar, and P. Tekasakul, "Computational fluid dynamic analysis of innovative design of solar-biomass hybrid dryer: an experimental validation," *Renewable Energy*, vol. 92, pp. 185–191, 2016.

[29] P. Demissie, M. Hayelom, A. Kassaye, A. Hailesilassie, M. Gebrehiwot, and M. Vanierschot, "Design, development and CFD modeling of indirect solar food dryer," *Energy Procedia*, vol. 158, pp. 1128–1134, 2019.

[30] Y. Amanlou and A. Zomorodian, "Applying CFD for designing a new fruit cabinet dryer," *Journal of Food Engineering*, vol. 101, no. 1, pp. 8–15, 2010.

[31] S. Khaldi, A. N. Korti, and S. Abboudi, "Applying CFD for studying the dynamic and thermal behavior of solar chimney drying system with reversed absorber," *International Journal of Food Engineering*, vol. 13, no. 11, pp. 1–20, 2017.

[32] M. Iranmanesh, H. Samimi Akhijahani, and M. S. Barghi Jahromi, "CFD modeling and evaluation the performance of a solar cabinet dryer equipped with evacuated tube solar collector and thermal storage system," *Renewable Energy*, vol. 145, pp. 1192–1213, 2019.

[33] S. Anand, D. P. Mishra, and S. K. Sarangi, "CFD supported performance analysis of an innovative biomass dryer," *Renewable Energy*, vol. 159, pp. 860–872, 2020.

[34] A. Benhamza, A. Boubekri, A. Atia et al., "Multi-objective design optimization of solar air heater for food drying based on energy, exergy and improvement potential," *Renewable Energy*, vol. 169, pp. 1190–1209, 2021.

[35] K. Nidhul, S. Kumar, A. K. Yadav, and S. Anish, "Computational and experimental studies on the development of an energy-efficient drier using ribbed triangular duct solar air heater," *Solar Energy*, vol. 209, pp. 454–469, 2020.

[36] Z. Alimohammadi, H. Samimi Akhijahani, and P. Salami, "Thermal analysis of a solar dryer equipped with PTSC and PCM using experimental and numerical methods," *Solar Energy*, vol. 201, pp. 157–177, 2020.

[37] E. Getahun, M. A. Delele, N. Gabbiye, S. W. Fanta, P. Demissie, and M. Vanierschot, "Importance of integrated CFD and product quality modeling of solar dryers for fruits

and vegetables: a review," *Solar Energy*, vol. 220, pp. 88–110, 2021.

[38] S. Misha, S. Mat, M. H. Ruslan, K. Sopian, and E. Salleh, "The prediction of drying uniformity in tray dryer system using CFD simulation," *International Journal of Machine Learning and Computing*, vol. 3, no. 5, pp. 419–423, 2013.

[39] Q. Luo, B. Li, Z. Wang, S. Su, and H. Xiao, "A study of unidirectional spiral tube for air evacuation in a solar heater with phase-change material," *Journal of Building Engineering*, vol. 46, Article ID 103659, 2022.

[40] S. P. Shetty, N. Madhwesh, and K. Vasudeva Karanth, "Numerical analysis of a solar air heater with circular perforated absorber plate," *Solar Energy*, vol. 215, pp. 416–433, 2021.

[41] A. Sanghi, R. P. K. Ambrose, and D. Maier, "CFD simulation of corn drying in a natural convection solar dryer," *Drying Technology*, vol. 36, no. 7, pp. 859–870, 2017.

[42] O. S. Idowu, O. M. Olarenwaju, and O. I. Ifedayo, "Determination of optimum tilt angles for solar collectors in low-latitude tropical region," *International Journal of Energy and Environmental Engineering*, vol. 4, no. 1, p. 29, 2013, http://www.journal-ijeee.com/content/4/1/29.